Numerical Research on the Impacts of Composite Panel Ballistic Using Perforated Plate for Combat Vehicle

Bakri Bakri(✉), Muhammad Syaiful Fadly, Khairil Anwar, Sri Chandrabakty, Mustafa, Naharuddin, and Fauzan

Department of Mechanical Engineering, Faculty of Engineering, University of Tadulako, Palu, Indonesia
muhsyaifulfadly@gmail.com

Abstract. In this research, a layered composite that utilizes a perforated plate was developed as a bullet-resistant material that works by breaking the tip of the projectile at the beginning of penetration and reducing the weight of the material. A Composite configuration with 3 layers with a steel plate was used as the first and third layers, while rubber was used in the second layer. Numerical modeling was developed using Ansys Workbench by varying the projectile penetration position on the perforated plate mounted on the front layer. Whereas, the Johnson–Cook material model was used in projectile and steel plate modeling, and the Mooney-Rivlin material model was used in rubber modeling. The outcome of the simulation showed that the position of the projectile penetration on the perforated plate affected the ballistic resistance in terms of the deformation and stress that occurred during the penetration. The deformation created a back bulge that got bigger as it held up the projectile velocity. The highest stress was found in the projectile penetration at the hole center (663 MPa), followed by the one at the side of the hole (623 MPa) and in the middle of four holes (593 MPa).

Keywords: Composite panel · Numerical modeling · Ballistic impact · Projectile

1 Introduction

Combat vehicles are made of steel to protect drivers and passengers from ballistic projectile shots [1, 2]. Steel has a heavy structure that interferes with the acceleration of the vehicles. The development of bullet-resistant materials for armored vehicles needs to be concerned in carrying out military attack and defense missions [3–6]. The development, mobility, and speed of armored vehicles are prime aspects of combat. Lighter vehicle weight allows faster acceleration or better agility in maneuvering [1, 6]. Armored vehicles should be able to provide protection from ballistic attacks with lightweight. Therefore, the development of bullet-resistant materials to handle various threats on the battlefield is effectively carried out and evaluated.

Bullet-resistant materials with high-impact loads at high velocity continue to be researched to seek potent materials, heat and surface treatment, and the manufacture of

N. I. Inda et al. (Eds.): ISST 2022, APR 7, pp. 15–25, 2023.
https://doi.org/10.2991/978-94-6463-228-6_3

coated materials with metallic and non-metallic materials [7–10]. Steel has been widely used as economical machine construction material in comparison to other materials, and it has better structural strength. Various developments are continuously carried out to invent bulletproof material technology that is lightweight but has optimal ballistic impact performance [11, 12]. The interest in the use of perforated plates to improve ballistic resistance has increased. Perforated plates can be used on armored vehicle bodies to reduce the total weight of the vehicle. The Perforated plate also induces bending stress of the projectile penetration [13].

Balos et al. [13] tried to optimize the use of materials, geometry, and the use of perforated plates, and they found that the perforated plate successfully prevented the projectile from penetrating the base plate, with a mass effectiveness value of 5.91. Bovrik et al. [14] used five high-strength sheets of steel to provide protection against 7.62 mm AP projectiles. Ballistic tests were used in determining the ballistic limits of those different steels. Mishra et al. [15] also carried out ballistic tests with 7.62 mm AP projectiles on steel plates that had been heating treated in different temperature variations ranging from 200 °C to 600 °C. Tests were also carried out on 5 mm perforated plates. The results show that the microstructure of the ballistic impact area has cracks by the induction of the adiabatic shear bands at tempering temperatures up to 400 °C. The holes in the plate also inhibited the adiabatic shear band formation.

The modeling of the projectile penetration on the target material at very high velocity can be done using a numerical model. The projectile velocity during penetration, distribution of von Mises stress on projectile and target and energy absorption can be estimated in numerical simulation. Yefa Hu et al. [16] examined the low-velocity impact behavior of carbon fiber-reinforced plastic beams using finite element simulation through LS-DYNA software. Energy absorption and target response to impact loads were investigated and compared with the ones of steel materials. Unfortunately, research on the combination between a perforated plate and rubber as an impact absorber against the high-velocity impact of projectiles that considers parameters such as deformation, von Mises stress and strain, and the response characteristics of perforated plates to projectile penetration were limited. In this research, the effect of the projectile penetration position on the perforated plate was measured in numerical simulation.

2 Material and Methods

In this research, composite panels made of 3 mm in thickness of steel plate on the outer layer and 4 mm in thickness of rubber on the middle layer were employed. The dimension of the panel was 150 × 150 mm. The front layer of the plate was made with a pattern of 3 mm holes in diameter and a gap between holes is 10 mm. Each layer of the material was unified using bolts which arrangement is presented in Fig. 1.

The ballistic testing of composite panels employed numerical simulation using ANSYS Workbench 15.0 software on explicit dynamics modeling. The meshing of the composite panels had tetrahedron shapes which were divided into two, coarse meshing of 2 mm in size for the area far from the projectile impact and fine meshing with a size of 0.8 mm in a 20 mm radius on the projectile impact area. The projectile used in this research was a 9 mm caliber Full Metal Jacket (FMJ) with tin wrap in brass and 0.8 mm of mesh size as shown in Fig. 2.

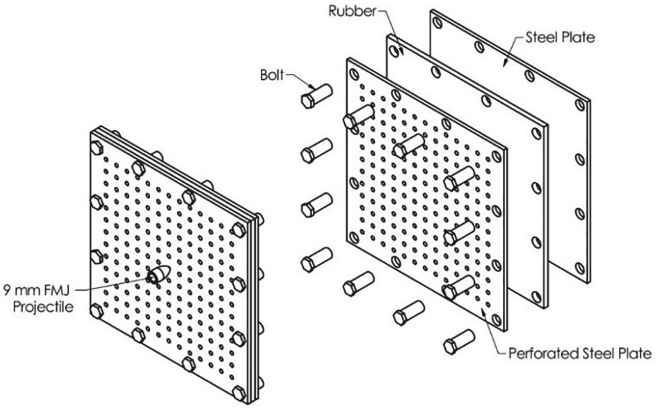

Fig. 1. The arrangement of the perforated plate, rubber, and plate

The initial projectile velocity was measured using the chronograph. The boundary condition was the fixed support on the outer side of the back plate. The target and projectile were modeled as a flexible body. Contact between the bodies was made frictionless. The time of the ballistic simulation was counted starting from when the initial bullet penetrated until the projectile stopped at 1.1 10–4 s. Stress and deformation were gained by adjusting the data solution information of the stress and deformation received by the composite panel during the impact process. The variables examined in this research included the position of the projectile penetration on the perforated plate in the center of the hole, the side of the hole, and the middle of four holes.

The Johnson–Cook material model was employed as the numerical simulation for projectiles and perforated plates and steel plates without holes. Johnson–Cook plasticity model includes strain rate, the strain effect, and temperature on flow stress [17–19]. Equation 1 shows the Johnson–Cook material model [20]. For rubber materials, the Mooney-Rivlin material model was used. This model can be used in materials that

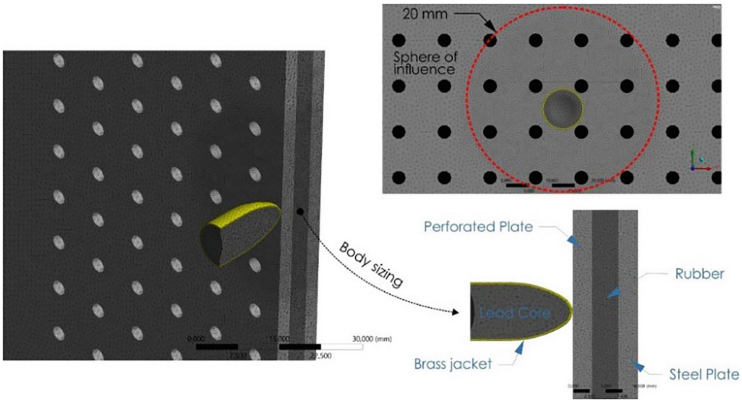

Fig. 2. Meshing model in numerical simulation

have large strains and are significantly non-linear. These behaviors include hyper-elastic deformability and incompressibility [21–23]. The Mooney-Rivlin general equation is shown in Eq. 2 [24, 25].

$$\sigma_{eq} = \left(A + B\varepsilon^{n}\right)\left(1 + C\ln\dot{\varepsilon}^{\circ}\right)\left(1 - \left(\frac{T - T_o}{T_{melt} - T_o}\right)^{m}\right) \tag{1}$$

where

σ_{eq} = equivalent stress (Pa)
A = yield stress constant (Pa)
B = hardening constant
ε = equivalent strain
n = hardening exponent
C = strain rate constant
m = thermal softening exponent
$\dot{\varepsilon}^{\circ}$ = plastic strain rate
T = test temperature (K)
T_o = room temperature (K)
T_{melt} = melting temperature (K)

$$\sigma_{eq} = 2C_1\left[D - \frac{1}{D^3}\right] + 2C_2\left[1 - \frac{1}{D^3}\right] \tag{2}$$

where

σ_{eq} = equivalent stress (Pa)
C_1, C_2 = probability constant (Pa)
D = extension ratio (Pa)

The properties of projectile and plate material according to the plasticity model of Johnson–Cook can be seen in Table 1. While, the rubber material properties are based on the Mooney-Rivlin model, as shown in Table 2.

3 Result and Discussion

Projectile penetration on composite panels can be examined in a simulation. Numerical simulation can determine the stress distribution, stress concentration, and deformation processes during impact events. Validation can be done by conducting ballistic testing to determine the accuracy. Simulation and experimental comparison results show similarities in terms of changes in the direction of the projectile when it penetrated the hole that hit the side of the hole as shown in Fig. 3 and Table 3.

$$\text{Error} = \left|\frac{4.588 - 4.534}{4.588}\right| \times 100\% = 1.17\% \tag{3}$$

The results of the ballistic impact measurements showed 98.82% similarity and an error rate of 1.17%. The validation test showed a small error value between numerical

Table 1. Johnson–cook material properties for projectiles and steel plates

Parameter	Unit	Brass Jacket	Lead Core	Steel Plate
Density	kg/m^3	8520	10,660	8859
Isotropic Elasticity				
Young Modulus	Pa	1.15×10^{11}	1×10^9	2×10^{11}
Poisson's Ratio	-	0.31	0.42	0.30
Johnson–Cook Plasticity				
Initial Yield Stress, A	Pa	2.06×10^8	2.4×10^7	1.467×10^8
Hardening Constant, B	Pa	5.05×10^8	3×10^8	8.969×10^8
Hardening Exponent, N	-	0.42	1	0.32
Strain Rate Constant, C	-	0.01	0.1	0.033
Thermal Softening Exponent, M	-	1.68	1	0.323
Melting Temperature, T_m	K	1189	760	1773
Reference Strain Rate	1/s	0.0005	0.0005	1

Table 2. Material properties based on Mooney Rivlin model parameters for rubber

Material	Density, kg/m^3	Material constant, C10 (Pa)	Material Constant, C01 (Pa)	Material Constant, C20 (Pa)	Material Constant, C11 (Pa)	Material Constant, C02 (Pa)	Incompressibility Parameter, D1 (1/Pa)
Rubber	1000	-4.5×10^5	7×10^5	1.6×10^6	2.5×10^6	-8×10^5	1×10^{-9}

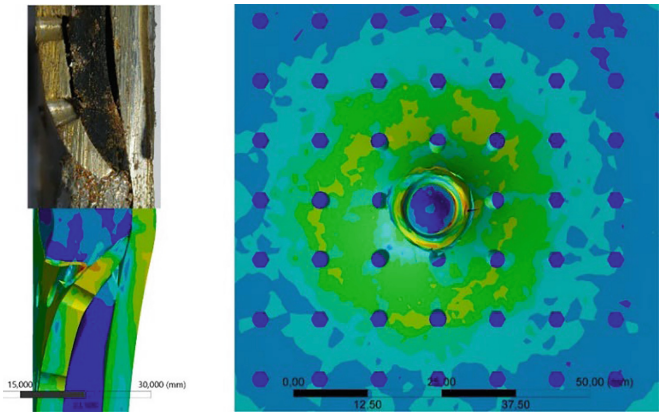

Fig. 3. Projectile penetration on composite panels by numerical simulation and experiments

Table 3. Comparison between numerical simulation and experimental results

Variable	Numerical Simulation	Experimental
Mass projectile	0.008 kg	0.008 kg
Velocity Projectile	365 m/s	365 m/s
Kinetic Energy	532.9 J	532.9 J
Bulge	4.534 mm	4.588 mm

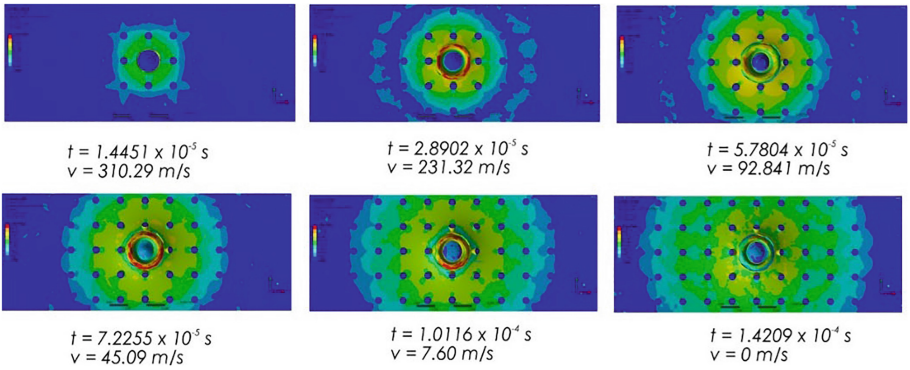

Fig. 4. Von mises stress: center of hole (front view)

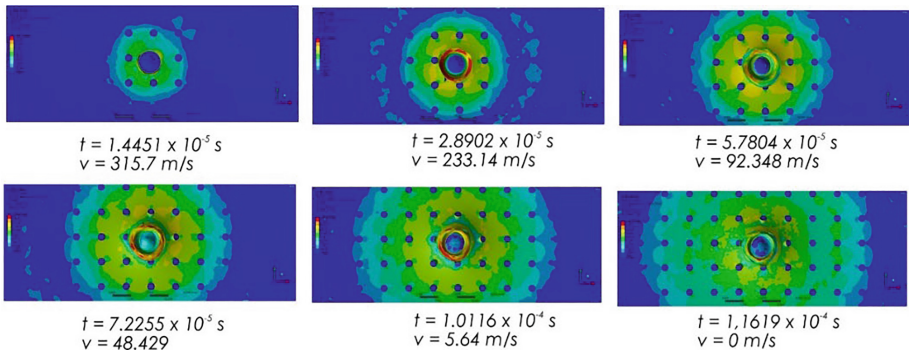

Fig. 5. Von mises stress: side of hole (front view)

and experimental simulations thereby numerical simulations with the finite element method can be used for impact ballistic examination on perforated plates. Three cases

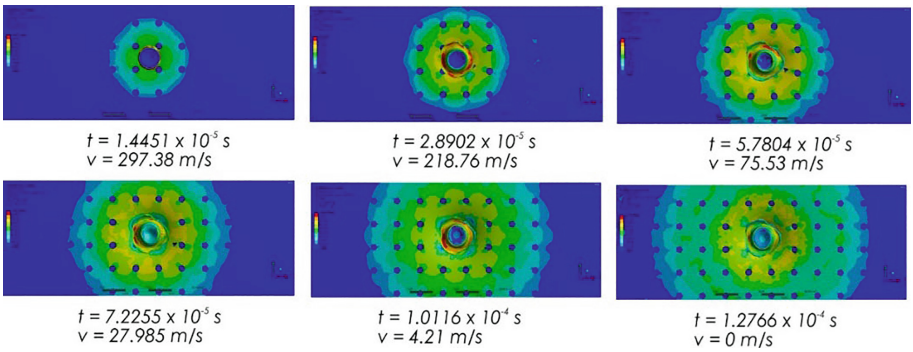

Fig. 6. Von Mises stress: middle of four holes (front view)

of projectile penetration at the center of the hole (Fig. 4), the side of the hole (Fig. 5), and the middle of four holes (Fig. 6) were examined in numerical simulation.

Projectile penetration on perforated plate distributed stress during the impact on the target and projectile. The hemispherical shape of the projectile became blunt and the plate started to perforate from the beginning of the impact. The maximum stress of the projectile was shown by the color change to red. The brass jacket on the projectile showed greater deformation with a stress value of 773.98 MPa when it penetrated the center of the hole at 2.8902×10^{-5} s (Fig. 4) compared to other penetration positions. The stress distribution was transferred throughout the target area of the composite panel until the projectile stopped. The projectile stopped faster when it penetrated the middle of four holes at 1.2766×10^{-4} s. The kinetic energy of the projectile when it penetrated the target material caused the material to deform and form a bulge on the back plate. The bulge pattern that appeared on the back plate is shown in Fig. 7.

During the impact event, the deformation got bigger while the projectile velocity decreased until the projectile stopped at 0 m/s. Projectile penetration in the center of the hole produced a larger bulge of 4.804 mm, at the side of the hole of 4.534 mm and the smallest bulge found in the middle of the four holes was 4.203 mm. Penetration in the center of the hole caused a bigger bulge effect because the projectile velocity resistance was zero. In the initial penetration, the projectile brass jacket peeled off when it penetrated the area around the hole. The slow decrease in projectile velocity resulted in a larger bulge than other penetration positions. The stresses that occurred during a ballistic impact event on a composite panel are shown in Fig. 8.

Figure 8 shows the stress distribution on the composite panels during a ballistic impact event. Projectile penetration in the center of the hole produced a greater maximum stress than in other penetration positions. The stress increased until it reached its maximum when the projectile perforated the target layer and fluctuated right before the projectile stopped. The maximum stress for composite panels when the projectile penetrated the center of the hole as 663 Mpa, 623 MPa at the side of the hole, and 593.52 MPa in the middle of four holes. The maximum stress made the penetration deeper. At the beginning of the penetration, the projectile started to deform due to contact with the front layer of the composite panel. Figure 9 shows the final deformation of the projectile.

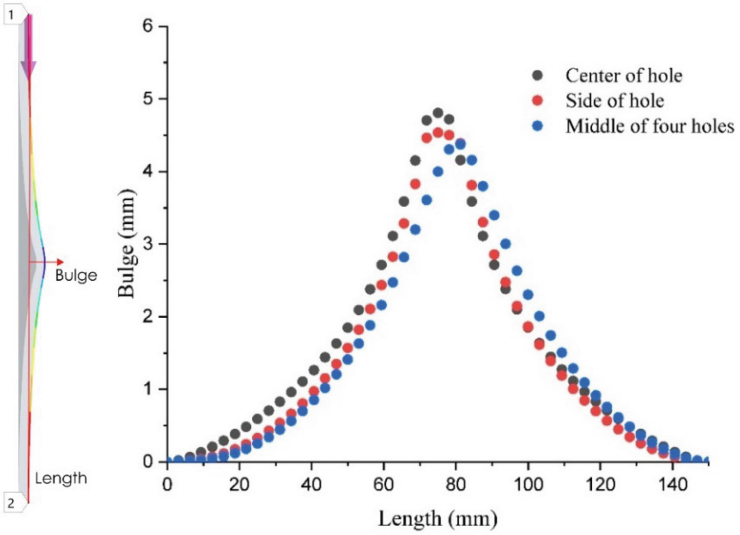

Fig. 7. Backplate bulge pattern due to ballistic impact

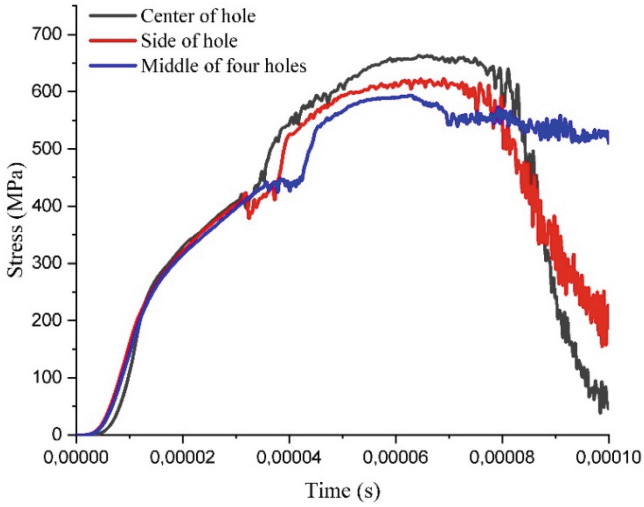

Fig. 8. Stress distribution vs time

Figure 9 shows that the largest projectile deformation was found then the projectile penetrated the middle of four holes. The projectile deformed faster and also stopped faster at a speed of 0 m/s, causing a smaller bulge on the back plate. In all cases, the penetration of the projectile in the perforated plate caused the projectile brass jacket to separate from the projectile core. The penetration position at the side of the hole (Fig. 9b) changed the angle of the final projectile each layer of the composite panel was perforated. The projectile angle has significantly deviated from the initial incident angle.

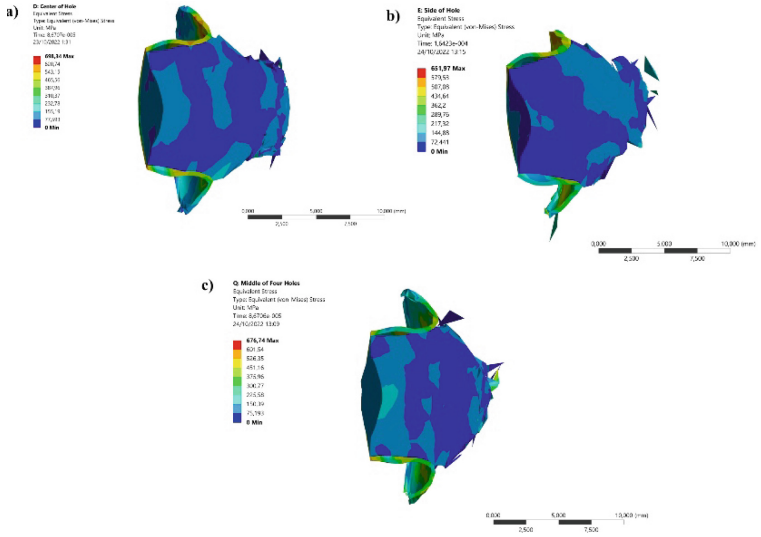

Fig. 9. Projectile deformation after ballistic impact: a) center of hole, b) side of the hole, c) middle of four holes

The mechanism of projectile failure, in this case, has been reported by Mishra et al. [15]. Figure 10 shows the penetration of the projectile at the end of the ballistic impact.

The rubber on each layer of the composite panel was torn due to the perforation on the perforated plate from projectiles. The rubber was perforated with a larger hole diameter at the end of the ballistic impact. Except at the penetration position of the middle of the four holes, the projectiles perforated the composite panel and stopped by the time they went into the last layer. The position in the center of the projectile hole perforated the first and second layers with insignificant deformation of the projectile causing a larger bulge on the back plate. Penetration at the side of the hole seemed to change the direction of the initial projectile incident, while in the middle of four holes, the projectile could not perforate every layer of the composite panel. The significantly deformed projectile made the rear plate bulge smaller.

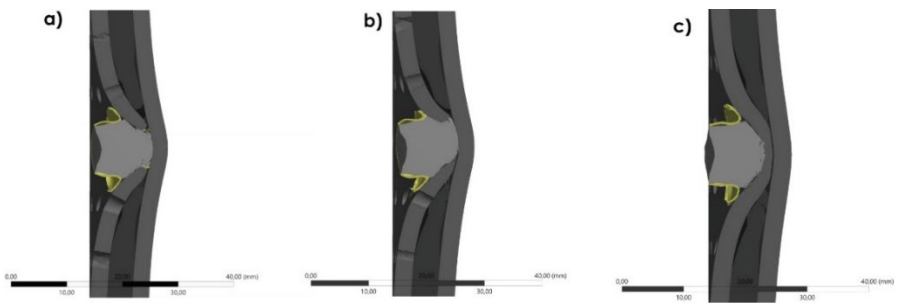

Fig. 10. Cross section of the projectile and composite panel at end of impact: a) center of hole, b) side of the hole, c) middle of four holes

4 Conclusion

The biggest bulge on the back plate and the maximum stress of 663 MPa on the composite panel occurred at the penetration position in the center of the hole of 4.804 mm. The position of the penetration at the side of the hole caused the direction of the projectile to change incidentally when it penetrated the perforated plate. The projectile punched holes in the first layer and tore off the rubber layer until the projectile stopped without successfully perforating the final layer. The penetration position in the middle of four holes resulted in a smaller bulge of 4.203 mm and a significant projectile deformation. The symmetrical pattern and the distance between the holes were greater than the diameter of the projectile, no side force caused the projectile to deviate from its initial trajectory.

Acknowledgements. We would like to thank the Faculty of Engineering, Tadulako University for funding to the sandwich composite panel for the resistance ballistic materials research project.

References

1. Hogg, P. J.: Composites for ballistic applications, Proc. Compos. Process, pp. 1–11 (2003).
2. Nayak, S. Y., et al.: Potential of natural fibers in composites for ballistic applications–a review, J. Nat. Fibers, vol. 19, no. 5, pp. 1648–1658 (2022).
3. Walley, S. M.: An introduction to the properties of silica glass in ballistic applications, Strain, vol. 50, no. 6, pp. 470–500 (2014).
4. Singh, B. B., Sukumar, G., Senthil, P.P., Jena, P.K., Reddy, P.R.S., Kumar, K.S., Madhu, V., Reddy, G.M.: Future armor materials and technologies for combat platforms, Def. Sci. J., vol. 67, no. 4, p. 412 (2017).
5. Jamil, W. N. M., Aripin, M.A., Sajuri, Z., Abdullah, S., Omar, M.Z., Abdullah, M.F., Zamri, W.F.H.: Mechanical properties and microstructures of steel panels for laminated composites in armored vehicles., Int. J. Automot. Mech. Eng., 13(3) (2016).
6. Madhu, V., Bhat, T. B.: Armour Protection and Affordable Protection for Futuristic Combat Vehicles., Def. Sci. J., 61(4) (2011).
7. Goda, I., Girardot, J.: A computational framework for energy absorption and damage assessment of laminated composites under ballistic impact and new insights into target parameters, Aerosp. Sci. Technol., 115, p. 106835 (2021).
8. Pereira, J. M., Lerch, B. A.: Effects of heat treatment on the ballistic impact properties of Inconel 718 for jet engine fan containment applications, Int. J. Impact Eng., 25(8), pp. 715–733 (2001).
9. Mondal, C., Mishra, B., Jena, P. K., Kumar, K. S., Bhat, T. B.: Effect of heat treatment on the behavior of an AA7055 aluminum alloy during ballistic impact, Int. J. Impact Eng., 38(8–9), pp. 745–754 (2011).
10. Atapek, S. H.: Ballistic impact behavior of quenched and tempered steels, in International Iron & Steel Symposium, pp. 413–419 (2012).
11. Yilmaz, A.: Development of armor steel for ballistic protection, Mater. Test., 52(11–12), pp. 811–818 (2010).
12. Siagian, J., Apriyanto, I. N. P., Djenod, K.: Development Of Steel As Anti-Ballistic Combat Vehicle Material, Soc. Sci. Res., 5(1), pp. 261–281 (2022).

13. Balos, S., Grabulov, V., Sidjanin, L., Pantic, M., Radisavljevic, I.: Geometry, mechanical properties and mounting of perforated plates for ballistic application, Mater. Des., 31(6), pp. 2916–2924 (2010).
14. Børvik, T., Dey, S., Clausen, A. H.: Perforation resistance of five different high-strength steel plates subjected to small-arms projectiles, Int. J. Impact Eng., 36(7), pp. 948–964 (2009).
15. Mishra, B., Jena, P. K., Ramakrishna, B., Madhu, V., Bhat, T. B., Gupta, N. K.: Effect of tempering temperature, plate thickness and presence of holes on ballistic impact behavior and ASB formation of a high strength steel, Int. J. Impact Eng., 44, pp. 17–28 (2012).
16. Hu, Y., Liu, C., Zhang, J., Ding, G., Wu, Q.: Research on carbon fiber–reinforced plastic bumper beam subjected to low-velocity frontal impact, Adv. Mech. Eng., 7(6), p. 1687814015589458 (2015).
17. Grytten, F., Børvik, T., Hopperstad, O. S., Langseth, M.: Low-velocity perforation of AA5083-H116 aluminum plates, Int. J. Impact Eng., 36(4), pp. 597–610 (2009).
18. Clausen, A. H., Børvik, T., Hopperstad, O. S., Benallal, A.: Flow and fracture characteristics of aluminum alloy AA5083–H116 as a function of strain rate, temperature and triaxiality, Mater. Sci. Eng. A, 364(1–2), pp. 260–272 (2004).
19. Johnson, G. R., Cook, W. H.: Fracture characteristics of three metals subjected to various strains, strain rates, temperatures and pressures, Eng. Fract. Mech., 21(1), pp. 31–48 (1985).
20. Johnson, G. R.: A constitutive model and data for materials subjected to large strains, high strain rates, and high temperatures, In: Proc. 7th Inf. Sympo. Ballist., pp. 541–547 (1983).
21. Helmy, P., Rudy, S., Anindito, P., Agus, S.: Energy absorbers on the steel plate-rubber laminate after deformable projectile impact, Восточно-Европейский журнал передовых технологий, 4(7)(94), pp. 6–12 (2018).
22. Khodadadi, A.: Numerical and experimental study of the impact on hyperelastic rubber panels, Iran. Polym. J., 28(2), pp. 113–122 (2019).
23. Aslam, M. A., Bin Rayhan, S., Yu, W. J.: Ballistic gelatin Lagrange Mooney-Rivlin material model as a substitute of bird in finite element bird strike case studies, Lat. Am. J. Solids Struct., 17 (2020).
24. Naarayan, S. S., Subhash, G.: Wave propagation in ballistic gelatine, J. Mech. Behav. Biomed. Mater., 68, pp. 32–41 (2017).
25. Ravikumar, N., Noble, C., Cramphorn, E., Taylor, Z. A.: A constitutive model for ballistic gelatin at surgical strain rates, J. Mech. Behav. Biomed. Mater., 47, pp. 87–94 (2015).